The Astrophysical Journal Supplement Series, 216:2 (9pp), 2015 January doi:10.1088/0067-0049/216/1/2

HYPERFINE-DEPENDENT gf-VALUES OF Mn I LINES IN THE 1.49–1.80 μm H BAND

M. Andersson[1,2], J. Grumer[3], N. Ryde[4], R. Blackwell-Whitehead[4],
R. Hutton[1,2], Y. Zou[1,2], P. Jönsson[5], and T. Brage[3]
[1] The Key Lab of Applied Ion Beam Physics, Ministry of Education, China
[2] Shanghai EBIT Laboratory, Modern Physics Institute, Fudan University, Shanghai, China; rhutton@fudan.edu.cn
[3] Division of Mathematical Physics, Department of Physics, Lund University, Sweden
[4] Department of Astronomy and Theoretical Physics, Lund University, Sweden
[5] School of Technology, Malmö University, Sweden
Received 2013 April 3; accepted 2014 July 28; published 2014 December 16

ABSTRACT

The three Mn I lines at 17325, 17339, and 17349 Å are among the 25 strongest lines ($\log(gf) > 0.5$) in the H band. They are all heavily broadened due to hyperfine structure, and the profiles of these lines have so far not been understood. Earlier studies of these lines even suggested that they were blended. In this work, the profiles of these three infrared (IR) lines have been studied theoretically and compared to experimental spectra to assist in the complete understanding of the solar spectrum in the IR. It is shown that the structure of these lines cannot be described in the conventional way using the diagonal A and B hyperfine interaction constants. The off-diagonal hyperfine interaction not only has a large impact on the energies of the hyperfine levels, but also introduces a large intensity redistribution among the hyperfine lines, changing the line profiles dramatically. By performing large-scale calculations of the diagonal and off-diagonal hyperfine interaction and the gf-values between the upper and lower hyperfine levels and using a semi-empirical fitting procedure, we achieved agreement between our synthetic and experimental spectra. Furthermore, we compare our results with observations of stellar spectra. The spectra of the Sun and the K1.5 III red giant star Arcturus were modeled in the relevant region, 1.73–1.74 μm, using our theoretically predicted gf-values and energies for each individual hyperfine line. Satisfactory fits were obtained and clear improvements were found using our new data compared with the old available Mn I data. A complete list of energies and gf-values for all the $3d^5 4s(^7S)4d$ e^6D – $3d^5 4s(^7S)4f$ w^6F hyperfine lines are available as supporting material, whereas only the stronger lines are presented and discussed in detail in this paper.

Key words: atomic data – infrared: stars – line: identification – methods: laboratory: atomic – methods: numerical – stars: abundances

Supporting material: machine-readable table

1. INTRODUCTION

High wavelength resolution spectrographs on satellite-borne and ground-based telescopes can resolve many of the absorption features in stellar spectra. In particular, line broadening effects such as hyperfine structure (HFS) and isotope shifts can be observed in the spectra of the Sun (Livingston & Wallace 1991) and other stars (e.g., Arcturus; Hinkle et al. 1995a). HFS increases the line width and decreases the peak intensity of the line profile. Omitting such effects will introduce an error in the measurement of the wavelength and the derived abundance from a stellar spectrum (Prochaska & McWilliam 2000). Jomaron et al. (1999) showed that if the HFS is not taken into account, the abundance of manganese in HgMn stars can be overestimated by up to three orders of magnitude. It was also shown that if the HFS of manganese is included as a crude estimate, the derived abundance may still be up to four times too large. Jomaron et al. (1999) suggested that the lack of accurate information about the HFS structure is the largest factor contributing to the uncertainty when estimating the abundance of manganese.

Hyperfine splitting of Mn I line profiles can be observed in the visible (Abt 1952) and infrared (Swensson 1966) spectrum of the Sun. In particular, Meléndez (1999) used the hyperfine split solar line profiles of Mn I in the H band (1.49–1.80 μm) and J band (1.00–1.34 μm) to measure the wavelength of the hyperfine component lines for the study of metal-rich stars in the Galactic bulge. However, Meléndez (1999) notes that the strong ($\log(gf) > -0.5$) Mn I lines at 17325, 17339, and 17349 Å have broad hyperfine splitting and appear to be blended with unknown features in the solar spectrum. Fitting these profiles is particularly difficult because there are no HFS constants in the literature for the upper levels ($3d^5 4s(^7S)4f$ w^6F_J) of these transitions. Furthermore, the fine structure energy level values for w^6F_J are poorly known and the National Institute of Standards and Technology (NIST) atomic level database (Ralchenko et al. 2008) provides values from the work of Catalan et al. (1964) who used the Landé interval rule to calculate the energy level values from blended transitions in the UV. The high uncertainty in the energy level values for w^6F_J increases the uncertainty in the line identification and thus the fitting of the blended infrared (IR) transitions. The laboratory line list for Mn I transitions in the IR by Taklif (1990) includes wavelengths for the 17325, 17339, and 17349 Å lines, but Meléndez (1999) misinterprets the Taklif (1990) line list and identifies the 17325 Å feature as only the $3d^5 4s(^7S)4d$ $e^6D_{9/2}$–$3d^5 4s(^7S)4f$ $w^6F_{9/2}$ transition. However, Taklif (1990) identifies the 17325 Å line as a blend of three transitions, $e^6D_{9/2}$–$w^6F_{9/2}$, $e^6D_{9/2}$–$w^6F_{7/2}$, and $e^6D_{9/2}$–$w^6F_{11/2}$. A similar misinterpretation is given by Meléndez (1999) for the 17339 and 17349 Å features, which are reported by Taklif (1990) to be the following blended lines: $e^6D_{7/2}$–$w^6F_{9/2,7/2,5/2}$ (17339 Å) and $e^6D_{5/2}$–$w^6F_{7/2,5/2,3/2}$ (17349 Å).

A high-resolution study of the spectrum of neutral manganese from the IR to the vacuum UV was reported in the thesis by Blackwell-Whitehead (2003), and further studies of the HFS

are given in Blackwell-Whitehead et al. (2005). It was noted in Blackwell-Whitehead (2003) that it was not possible to fit the transitions from the w^6F term using diagonal hyperfine interaction constants. In this work, Blackwell-Whitehead also indicated that the hyperfine splitting of the blended 17325, 17339, and 17349 Å lines may require a more detailed theoretical analysis to fully understand these line profiles. Furthermore, given that the 17325, 17339, and 17349 Å lines are within the 25 strongest ($\log(gf) > -0.5$) Mn I lines in the *H* band, a study of their profiles will assist in a complete interpretation of the solar spectrum in the IR.

We show that the 17325, 17339, and 17349 Å line features are hyperfine-split blended features of the $e^6D_{9/2}$–w^6F, $e^6D_{7/2}$–w^6F, and $e^6D_{5/2}$–w^6F transitions. These features cannot be described using diagonal hyperfine interaction constants due to a strong off-diagonal hyperfine interaction, which in some cases leads to such a large mixing between the hyperfine levels that the *J*-quantum number loses its meaning. Thus, to assist in the analysis of these transitions in stellar spectra, we provide individual relative line positions and *gf*-values for each hyperfine transition. Furthermore, we suggest that the solar line profiles for 17325, 17339, and 17349 Å (air wavelengths) can be explained by off-diagonal hyperfine interaction, and we claim that these lines are not significantly affected by unknown blends in the solar spectrum. These lines should therefore be useful in the analysis of stellar spectra, for instance in the determination of stellar Mn abundances.

2. HYPERFINE INTERACTION

In isotopes with a non-zero nuclear spin, *I*, there is an interaction between the electromagnetic moments of the nucleus and the electrons that is often referred to as the hyperfine interaction. This interaction couples the total electronic angular momentum *J* and the nuclear spin *I* to a new total angular momentum *F*. As a consequence of this interaction, each fine structure level is split up into several closely spaced hyperfine levels. If the energy separations between the fine structure levels are large compared to the separations due to the hyperfine interaction, the energies of the hyperfine levels can be calculated using the lowest-order perturbation theory

$$E_{\rm hpf}(\gamma JF) = E_{fs}(\gamma J) + \frac{1}{2}AK + B\frac{(3/4)K(K+1) - J(J+1)I(I+1)}{2I(2I-1)J(2J-1)}, \quad (1)$$

where $E_{fs}(\gamma J)$ is the energy of the fine structure level,

$$K = F(F+1) - J(J+1) - I(I+1), \quad (2)$$

and *A* and *B* are the hyperfine interaction constants. The label γ denotes the quantum numbers required to identify the fine structure level.

Manganese has only one stable isotope, with a nuclear spin of $I = 5/2$ and a strong nuclear magnetic dipole moment, $\mu_I = 3.4687$ nuclear magnetons, as well as a small electric quadrupole moment, $Q = 0.32$ barns (Lide 2003), leading to a potentially strong hyperfine interaction. The open $4s$ shell in the $3d^5 4s(^7S)4f\,w^6F$ term gives rise to a strong hyperfine interaction. At the same time the fine structure of this term is very small, resulting in a strong off-diagonal hyperfine interaction, i.e., interaction between hyperfine levels derived from different fine structure levels described in the diagonal approximation using the *A* and *B* interaction constants.

In order to describe a system where the fine and HFS energy splitting is of the same order of magnitude, one has to use higher orders of perturbation calculations or use a matrix formalism to take the off-diagonal hyperfine interaction into account. In this work, we have used the latter approach. We will not describe the method in detail in this paper, but we refer to three earlier papers that were based on similar approaches, Andersson et al. (2006), Grumer et al. (2010), and Andersson et al. (2012).

To describe the hyperfine states, we couple the *J*-dependent electronic wave function $|\gamma J\rangle$ to the nuclear wave function $|I\rangle$ using standard coupling theory to build *F*-dependent wave functions $|\gamma JIF\rangle$ (FSF), which form a set of basis functions in our calculation. The Atomic State Function (ASF), $|\Gamma F\rangle$, representing the hyperfine mixed levels, is written as a linear combination of the FSFs as

$$|\Gamma F\rangle = \sum_i c_i |\gamma_i J_i I F\rangle, \quad (3)$$

where c_i are the expansion coefficients.

In the calculation of the lower hyperfine levels, all possible $|e^6DJIF\rangle$ and $|e^8DJIF\rangle$ FSFs were used, and for the upper hyperfine levels, all $|w^6FJIF\rangle$ and $|w^8FJIF\rangle$ were used. Using these basis functions, the hyperfine interaction Hamilton matrix was set up and diagonalized to yield hyperfine level energies and the expansion coefficients of the ASFs.

The transition operator acts only on the electronic part of the wave function and the nuclear part can therefore be decoupled. The gf-values of the hyperfine transitions can then be calculated in terms of *J*-dependent transition matrix elements as

$$gf = \frac{8\pi^2 m_e c a_0^2 \sigma}{3h}(2F_i+1)(2F_j+1) \times \left| \sum_i \sum_j (-1)^{J_i} c_i c_j \begin{Bmatrix} F_i & J_i & I \\ J_j & F_j & 1 \end{Bmatrix} \langle \gamma_i J_i \| \mathbf{D}^{(1)} \| \gamma_j J_j \rangle \right|^2. \quad (4)$$

For details, see Grumer et al. (2010).

3. METHOD OF CALCULATION

In the calculations, we first optimized the wave functions for the lower e^6D_J and the upper w^6F_J fine structure levels using the relativistic atomic structure package Grasp2K (Jönsson et al. 2013). These programs are based on the multiconfiguration Dirac-Hartree-Fock method as outlined by Grant (2007). The even and the odd states were optimized in two separate calculations. Using the electronic wave functions, the Hamiltonian matrix, including the hyperfine interaction, was constructed and diagonalized using the Hfszeeman program (Andersson & Jönsson 2008) to give the hyperfine level energies as well as the corresponding wave functions in the form of Equation (3).

Using the ASFs for the hyperfine levels, the gf-values of the transitions were calculated using a newly developed code, connected to the Grasp2K suite of programs, that determines rates of *F*-dependent transitions in a general manner (J. Grumer et al., in preparation). Note that this code also allows for an external magnetic field in cases when it is large enough to be nonnegligible. The program is based on Equation (4) and uses the mixing coefficients from Hfszeeman together with the *J*-dependent transition matrix elements from a slightly modified version of the Grasp2K transition program.

To investigate the importance of the off-diagonal hyperfine interaction, two different calculations were performed. The first we named the *Complete* calculation and the second the *Diagonal* calculation. In the *Complete* calculation, the full hyperfine interaction matrix was used, whereas in the *Diagonal* calculation only the diagonal hyperfine interaction matrix elements were included. The *Diagonal* calculation therefore corresponds to describing the hyperfine interaction in terms of A and B hyperfine interaction constants.

4. LABORATORY MEASUREMENTS

The emission spectrum of manganese, Figures 2–4, was recorded at the NIST with the NIST 2 m Fourier transform spectrometer (Nave et al. 1997) using resolutions of 0.008 to 0.03 cm^{-1}, which is sufficient to fully resolve the Doppler broadened line profiles of the transitions. The light source used was a water-cooled hollow cathode lamp (Blackwell-Whitehead 2003; Blackwell-Whitehead et al. 2005). Owing to the brittle nature of pure manganese, the cathodes were made of an alloy of 95% Mn and 5% Cu. The hollow cathode was run at a current of 1.5 A, with 1.9 Torr of Ne as a buffer gas.

5. SYNTHETIC SPECTRA

The laboratory spectra were recorded using a hollow cathode, and the line intensities of a spectrum from such a light source should be proportional to the gf-values under the assumptions that the transition rates are much higher than the collision rates and that line intensities from the same multiplet are compared. The synthetic spectra were generated by giving each hyperfine line a Voigt profile, and the FWHM was fitted to the experimental spectrum.

To be able to reproduce the experimental spectrum, it was necessary to adjust our ab initio energies. The energies of the e^6D levels were determined experimentally, but the fine structure of the w^6F term is poorly known. The NIST atomic level database (Ralchenko et al. 2008) provides values from the work of Catalan et al. (1964), who used the Landé interval rule to calculate the energy level values from blended transitions in the UV. However, since the hyperfine interaction is of the same order as the fine structure splitting, this method should be considered invalid.

Starting from accurate fine structure energies is of great importance since the hyperfine mixing is very sensitive to the fine structure splitting. The fine structure splitting of the w^6F levels is very small compared to the term splitting between w^6F and $3d^5 4s(^7S)4f\ z^8F$. Since the fine structure is associated with the spin–orbit interaction and this interaction is responsible for the mixing between the levels of w^6F and z^8F, the fine structure of w^6F should be close to the Landé interval rule,

$$E_{fs}(LSJ) = \frac{\mathcal{C}(LS)}{2}[J(J+1) - L(L+1) - S(S+1)], \quad (5)$$

where $\mathcal{C}$ is the Landé interval constant. We used this argument as a starting point when trying to reproduce the experimental spectrum. Using the error defined by the least square fit between the synthetic and experimental spectra, the Landé interval constant was varied to find the best fit. The resulting value of $\mathcal{C}$ was in this case found to be 0.0150 cm^{-1}. We will refer to results using this method as *Landé Fitted*.

To further improve the fitting and allow for deviations from the Landé interval rule, the energies of the independent fine structure levels were varied. This was also performed using the error defined by the least square fit between the synthetic and experimental spectra. Using this approach, good agreement was found between the synthetic and experimental spectra. Results based on this model will be referred to as *Level Fitted*.

In general, even if theoretically predicted gf-values are close to experimental ones, the predicted energies of the lines are not of experimental accuracy. To improve our synthetic spectra, we therefore made a final adjustment where we allowed for small variations of the hyperfine level energies when fitting to experimental spectra. In these adjustments, only the hyperfine level energies were changed, whereas all gf-values were kept fixed. We again used the error defined by the least square fit between the synthetic and experimental spectra to find a better fit. We allowed for variations for both the lower and upper hyperfine levels, resulting in 54 free parameters. Our computer power was not large enough to handle so many parameters, but we had to try to improve the spectra stepwise, going from the upper to the lower end of the spectrum. Using this approach, we can reproduce the experimental spectrum with very high accuracy. We will refer to results including this final adjustment as *Hyperfine Adjusted*.

6. RESULTS AND DISCUSSION

Besides trying to reproduce the experimental spectra and obtaining information about all individual hyperfine lines, we also investigated the importance of the off-diagonal hyperfine interaction, and how important the different steps of our fitting procedure were to reproducing the experimental spectra. The influence of the off-diagonal hyperfine interaction can be found by comparing the results from *Diagonal* and *Complete* calculations (see Section 3).

Using the *Landé Fitted* method described in Section 5, we performed *Diagonal* and *Complete* calculations, trying to fit the synthetic spectra to the experimental spectra by varying the Landé interval constant. The former of these we will refer to as the *Diagonal* and the latter as the *Complete Landé Fitted* (*CLaF*) calculation. Comparing the spectra from these two calculations, we can determine the importance of the off-diagonal hyperfine interaction.

Including the off-diagonal hyperfine interaction, we performed two further calculations, the *Complete Level Fitted* (*CLeF*) using the *Level Fitted* procedure described in Section 5, and the *Complete Hyperfine Adjusted* (*CHA*) using the *Hyperfine Level Adjusted* method also described in Section 5.

Comparing the synthetic spectra from the *CLaF* calculation to those from the *CLeF* calculation, the influence of adjusting the fine structure energies of w^6F from the Landé interval rule can be determined. Finally, the impact of adjusting the individual hyperfine level energies to the synthetic spectra can be investigated by comparing the spectra from the *CLeF* calculation with the spectra from the *CHA* calculation.

To see how the synthetic spectra changed through the *Diagonal*, *CLaF*, *CLeF*, and *CHA* calculations, we have chosen to present the 17339 Å spectral feature, corresponding to the $e^6D_{7/2}$–w^6F hyperfine lines, for these four calculations in Figure 1. The differences between the four different synthetic spectra for the 17325, 17349, 17357, and 17362 Å spectral features, corresponding to the $e^6D_{9/2,5/2,3/2,1/2}$–w^6F hyperfine lines, follow much the same pattern.

From Figure 1 we found that the *Diagonal* calculation in principle predicts one strong peak surrounded on both sides by weak structure. The spectrum from the *CLaF* calculation predicts a much wider and more complex structure and there are in principle no similarities between the two spectra. It should

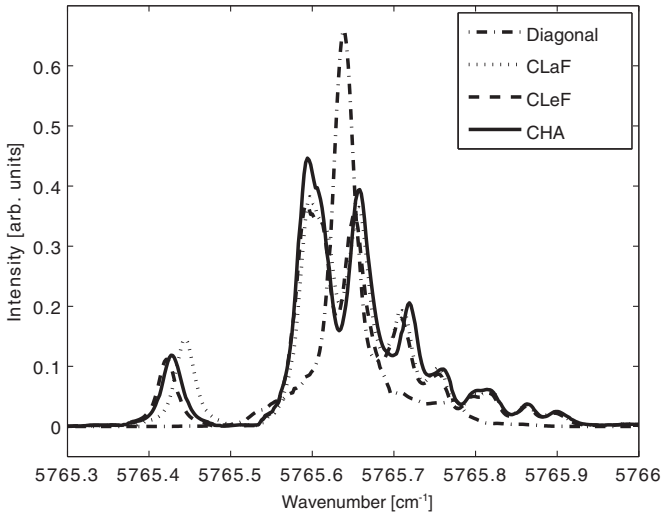

Figure 1. Four different synthetic spectra of the $e^6D_{7/2}$–w^6F transitions (the 17339 Å line). The dash–dotted spectrum is from the *Diagonal* calculation, the dotted from the *Complete Lande Fitted* calculation (*CLaF*), the dashed from the *Complete Level Fitted* (*CLeF*), and the solid from the *Complete Hyperfine Level Adjusted* (*CHA*).

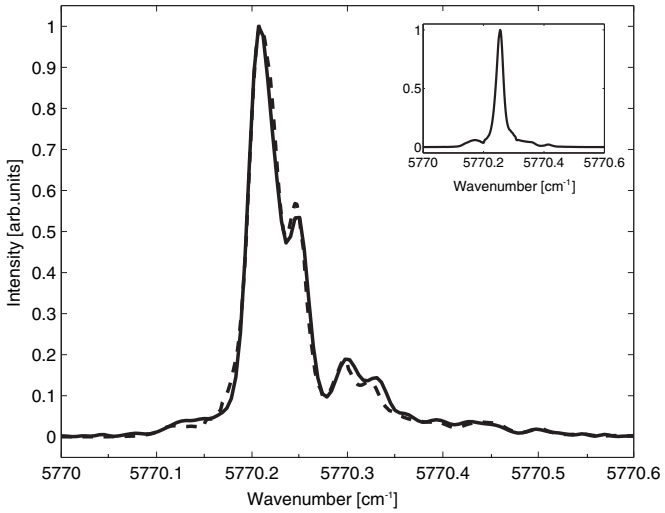

Figure 2. Experimental spectrum (solid line) compared to the *CHA* spectrum (dashed line) for the $e^6D_{9/2}$–w^6F transitions (the 17325 Å line). The *Diagonal* spectrum is presented as an inset plot.

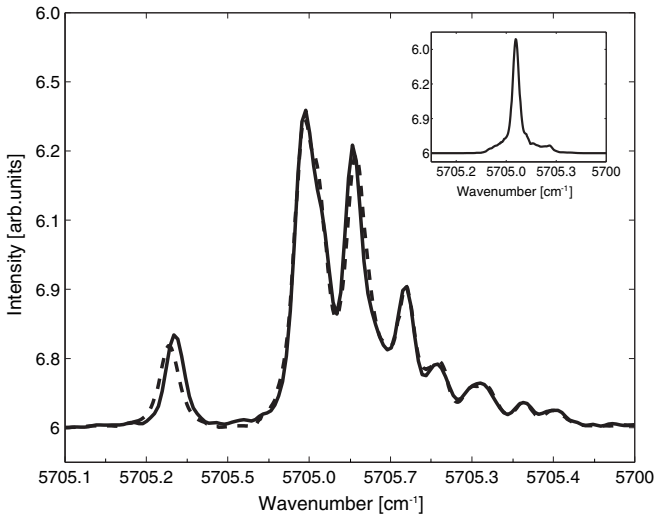

Figure 3. Experimental spectrum (solid line) compared to the *CHA* spectrum (dashed line) for the $e^6D_{7/2}$–w^6F transitions (the 17339 Å line). The *Diagonal* spectrum is presented as an inset plot.

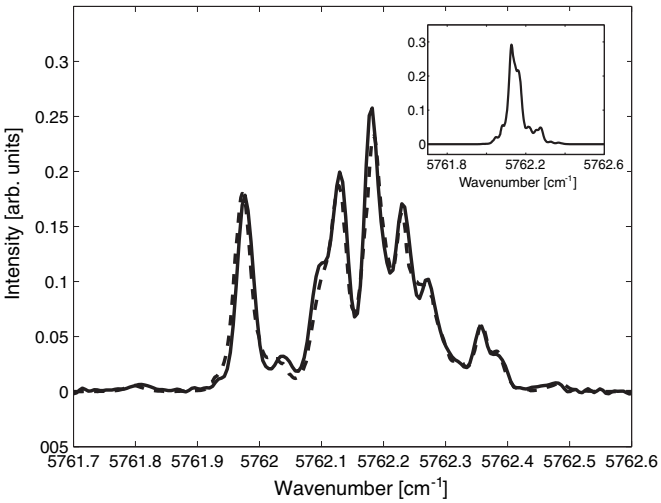

Figure 4. Experimental spectrum (solid line) compared to the *CHA* spectrum (dashed line) for the $e^6D_{5/2}$–w^6F transitions (the 17349 Å line). The *Diagonal* spectrum is presented as an inset plot.

be pointed out that these differences are entirely due to the off-diagonal hyperfine interaction, which not only affects the energies of the hyperfine levels, but also has a very large impact on the gf-values of the individual hyperfine transitions. It is clear from this picture that the hyperfine levels of w^6F cannot be described in terms of *A* and *B* hyperfine constants.

Moving from the *CLaF* to the *CLeF* spectrum, we found that the position and the intensities of some lines were slightly changed, but the differences are rather small. The same is found going from *CLeF* to *CHA*. It should be pointed out that going from *CLaF* to *CLeF* not only changed the position of the hyperfine lines, but also slightly changed the gf-values, whereas going to *CHA* only changed the position of the hyperfine lines and the gf-values were the same as for *CLeF*.

Below we give some results in detail for the three spectral regions of e^6D–w^6F of greatest astrophysical interest. For each group of peaks, we present a figure (Figures 2–4) where we have plotted our synthetic spectrum from the *CHA* calculation compared to the experimental one. In each figure we also present the synthetic spectrum from the *Diagonal* calculation as an inset plot.

The off-diagonal hyperfine interaction gives rise to many new transitions, and the total number of transitions within each sub-spectrum can therefore be very large; the total transition list is therefore too long to be published in the main article but is available as supporting material. Instead, we have chosen to present those lines that have a gf-value equal to or greater than 10% of the largest gf-value within each sub-spectrum. These lines give a good description of the spectrum and the additional lines only make small changes; the reduced list is therefore sufficient for discussing the results.

In each table, various information about each hyperfine line is presented. In the first column, the *F*-value of the w^6F hyperfine level is given. The second column is labeled HFS, and refers to the HyperFine State. This is an index identifying the different hyperfine levels in the calculations. Since the off-diagonal hyperfine interaction introduces a large amount of mixing between the hyperfine states in this system, the *J*-value

Table 1
Line List of the $e^6D_{9/2}$–w^6F Transitions (the 17325 Å line) Based on Theoretical Calculations

w^6F		e^6D		Complete		Diagonal	
F	HFS	F	HFS	Wave number (cm^{-1})[a]	gf[b]	gf	Δgf (%)
5	39	4	31	5770.2040	5.895	6.047	3
4	38	3	30	5770.2033	4.875	4.859	−0
3	37	2	29	5770.2047	3.999	3.916	−2
6	42	5	32	5770.2126	7.193	7.475	4
7	47	6	33	5770.2212	8.898	9.153	3
8	54	7	34	5770.2474	1.109×10^1	1.109×10^1	0
5	46	5	32	5770.2917	1.281	9.455×10^{-1}	−26
6	52	6	33	5770.2983	1.707	1.269	−26
7	61	7	34	5770.3259	2.219	1.692	−24

Notes. Only those with a gf-value of at least 10% of the largest gf-value have been included. HFS is a hyperfine level index. See Section 6 for discussions about the wavenumber and gf-value uncertainties.

[a] Our recommended wavenumbers with an estimated overall relative uncertainty less than $0.02\,cm^{-1}$.

[b] Our recommended gf-values with an estimated overall uncertainty of 5%.

(This table is available in its entirety in machine-readable form.)

is no longer a good quantum number and can therefore not be used to identify the hyperfine levels. Instead, we gave each hyperfine level an identification number according to the energy order of the hyperfine levels within each parity symmetry. In columns three and four, the corresponding information is given for e^6D hyperfine levels. In column five, the wavenumber from the *CHA* calculation for the hyperfine transition is given, and in the sixth column the *gf-value* from the same calculation is given. In column seven, the gf-value from the corresponding hyperfine transition in the *Diagonal* calculation is given, and in the last column is the difference in gf-value of the *Diagonal* calculation relative to the *CHA* calculation. The complete e^6D–w^6F line list can be found as supporting material.

The accuracy of the wavenumbers should undoubtedly be high, as the atomic energy structure is deduced from high-quality wavefunctions and subsequently anchored to high-precision laboratory spectra. The values in the tables are therefore given with four decimals. The estimated uncertainties of the relative positions, which are the important quantities here, are smaller than $\pm 0.02\,cm^{-1}$. This is better than what is required for stellar spectroscopy. It should be made clear that the uncertainties of the absolute wavenumbers are slightly higher, as they are dependent on the calibration of the experimental spectra.

6.1. The 17325 Å Line

We start by investigating the 17325 Å line corresponding to the $e^6D_{9/2}$–w^6F transitions in the interval 5770.0–5770.6 cm^{-1}. The result is presented as a plot in Figure 2 and in detail in Table 1. From Figure 2, we find that our *CHA* synthetic spectrum reproduces the features of the experimental one, whereas the *Diagonal* calculation predicts a structure that is too simple. The main differences between the *Diagonal* and the *CLeF* spectra are the two peaks emerging at 5770.30 cm^{-1} and 5770.33 cm^{-1}. From Table 1, we find that the predicted gf-values for the hyperfine transitions making up these lines are about 25% smaller in the *Diagonal* calculation than in the *CLeF* calculation. The fact that these two lines emerge in the spectrum generated from the *CLeF* calculation is only partly explained by the enhancement of the gf-values. The main underlying reason is rather the shift in energy induced by the off-diagonal hyperfine interaction.

6.2. The 17339 Å Line

The 17339 Å line is situated in the region 5765.3–5766.0 cm^{-1}. A comparison between the experimental and the *CHA* spectra is presented in Figure 3. In the same figure, the spectrum from the *Diagonal* calculation is also included as an inset plot. Starting with the *Diagonal* spectrum, we find that it in principle predicts only one peak, whereas the experimental spectrum of the $e^6D_{7/2}$–w^6F transitions is much more complex. The *CHA* synthetic spectrum, on the other hand, reproduces all features of the experimental one. The largest difference between the *CHA* and experimental spectra is the line at 5765.43 cm^{-1}. In *CHA*, this peak is approximately 10% lower than in the experimental spectrum, and it is positioned at an energy that is $0.007\,cm^{-1}$ too low.

The results are presented in detail in Table 2. It is found that there are much larger differences between the *Diagonal* and *CLeF* calculation for this part of the spectrum than for the 17325 Å spectral feature. Even the gf-values for the strongest and second strongest lines differ by 10% and 28%, respectively. Even more notable is that there are three lines in the list that have gf-values that are identically zero in the *Diagonal* calculation, and that the strongest of these have a gf-value that is 14% of the strongest of all lines in this part of the spectrum. It is clear from this list that the changes to the gf-values due to the off-diagonal hyperfine interaction have a very large impact on the spectrum.

6.3. The 17349 Å Line

The 17349 Å line is situated in the region 5761.7–5762.6 cm^{-1}. In the main plot of Figure 4, we compare our *CHA* synthetic spectrum to the experimental. The corresponding spectrum generated from the *Diagonal* calculation is presented as an inset plot. Comparing the *Diagonal* synthetic spectrum to the experimental, we find that it is far off the target and that there are not many similarities between the two spectra for the $e^6D_{5/2}$–w^6F transitions. However, there is a good resemblance between the *CHA* synthetic spectrum and the experimental one.

Table 2
Line List of the $e^6D_{7/2}$–w^6F Transitions (the 17339 Å Line) Based on Theoretical Calculations

w^6F		e^6D		Complete		Diagonal	
F	HFS	F	HFS	Wave number (cm^{-1})[a]	gf[b]	gf	Δgf (%)
5	39	4	38	5765.4221	8.493×10^{-1}	0	...
6	42	5	39	5765.4283	1.002	0	...
7	47	6	40	5765.4371	7.791×10^{-1}	0	...
3	41	2	36	5765.5891	2.563	2.704	5
4	43	3	37	5765.5901	2.884	3.650	27
5	46	4	38	5765.5943	3.574	4.831	35
2	40	1	35	5765.6043	2.212	1.991	−10
6	52	5	39	5765.6137	4.899	6.263	28
4	50	4	38	5765.6496	1.207	1.146	−5
7	61	6	40	5765.6579	7.160	7.964	11
5	56	5	39	5765.6728	1.967	1.753	−11
2	45	2	36	5765.6911	7.873×10^{-1}	4.918×10^{-1}	−38
6	64	6	40	5765.7191	3.196	2.595	−19
3	55	3	37	5765.7455	7.959×10^{-1}	6.942×10^{-2}	−91
5	56	4	38	5765.7597	8.283×10^{-1}	4.023×10^{-1}	−51
4	58	4	38	5765.7982	9.405×10^{-1}	6.545×10^{-2}	−93
5	65	5	39	5765.8638	7.462×10^{-1}	4.363×10^{-2}	−94

Notes. Only those with gf-values of at least 10% of the largest gf-value have been included. HFS is a hyperfine level index. See Section 6 for discussions about the wavenumber and gf-value uncertainties.
[a] Our recommended wavenumbers with an estimated overall relative uncertainty less than 0.02 cm^{-1}.
[b] Our recommended gf-values with an estimated overall uncertainty of 5%.

Table 3
Line List of the $e^6D_{5/2}$–w^6F Transitions (the 17349 Å Line) Based on Theoretical Calculations

w^6F		e^6D		Complete		Diagonal	
F	HFS	F	HFS	Wave number (cm^{-1})[a]	gf[b]	gf	Δgf (%)
5	46	4	45	5761.9605	1.632	0	...
4	43	3	44	5761.9661	1.428	0	...
6	52	5	46	5761.9707	1.265	0	...
3	41	2	43	5761.9790	8.594×10^{-1}	0	...
3	48	2	43	5762.0822	8.391×10^{-1}	1.720	105
4	50	3	44	5762.0904	1.217	2.627	116
2	45	1	42	5762.1138	1.319	1.032	−22
3	55	3	44	5762.1196	4.518×10^{-1}	6.925×10^{-1}	53
5	56	4	45	5762.1261	2.124	3.783	78
1	44	0	41	5762.1315	8.210×10^{-1}	5.350×10^{-1}	−35
4	58	4	45	5762.1431	1.309	1.484	13
6	64	5	46	5762.1700	3.845	5.216	36
3	55	2	43	5762.1840	7.301×10^{-1}	6.677×10^{-1}	−9
2	53	2	43	5762.1971	9.588×10^{-1}	2.473×10^{-1}	−74
5	65	5	46	5762.2039	3.043	2.720	−11
4	58	3	44	5762.2413	6.580×10^{-1}	6.595×10^{-1}	0
4	63	5	46	5762.2547	1.016	5.505×10^{-1}	−46
3	57	3	44	5762.2582	1.126	0	...
2	60	3	44	5762.2783	6.592×10^{-1}	1.802×10^{-1}	−73
5	65	4	45	5762.2958	4.375×10^{-1}	4.534×10^{-1}	4
4	63	4	45	5762.3559	8.882×10^{-1}	1.126×10^{-1}	−87
3	62	4	45	5762.3565	6.840×10^{-1}	3.378×10^{-1}	−51

Notes. Only those with a gf-value of at least 10% of the largest gf-value have been included. HFS is a hyperfine level index. See Section 6 for discussions about the wavenumber and gf-value uncertainties.
[a] Our recommended wavenumbers with an estimated overall relative uncertainty less than 0.02 cm^{-1}.
[b] Our recommended gf-values with an estimated overall uncertainty of 5%.

Inspecting the results of the $e^6D_{5/2}$–w^6F hyperfine transitions as presented in Table 3, it is found that the differences between the *CLeF* and *Diagonal* calculations are even larger than for the 173325 and 17339 Å spectral features in the spectrum. The transition with the largest gf-value differs by 36% between the two calculations, and the fourth strongest line, with a gf-value of 42% of the largest, in the *CHA* calculation is a strictly forbidden transition in the *Diagonal* calculation. Actually, the 4th, 5th, 8th, 10th, and 14th strongest lines of the 22 transitions in the line list are all induced by the off-diagonal hyperfine interaction and are absent in the *Diagonal* spectrum. This has of course a very large impact on the spectrum and is further proof of the

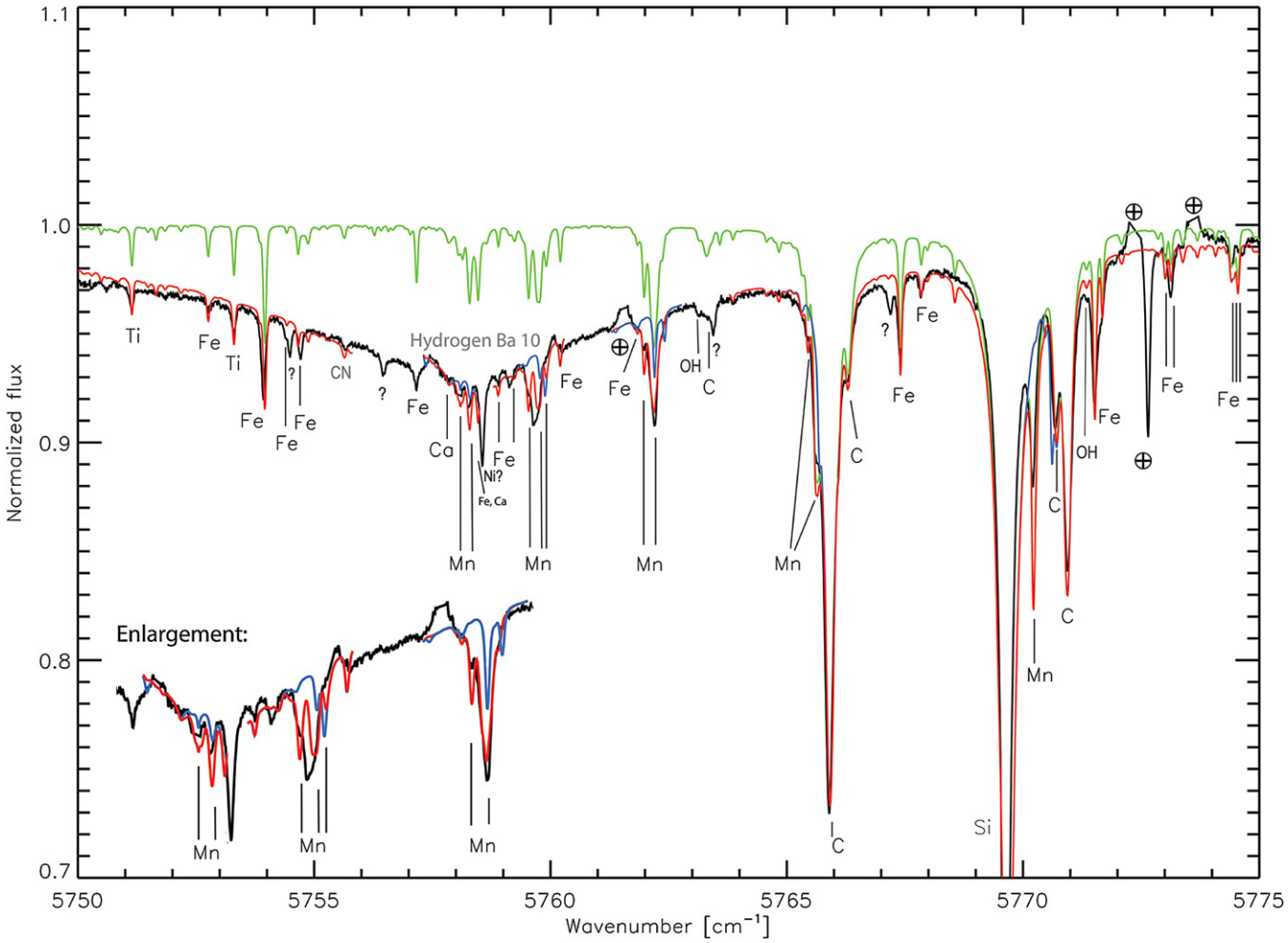

Figure 5. Section of the observed solar spectrum Livingston & Wallace (1991), shown in black. Our best synthetic spectra are shown in red, and include our newly calculated Mn lines. In green, we show the same spectrum, but omitting the Hydrogen Bracket 10 line to show its influence. The blue spectrum shows the spectrum using the Mn line list from the VALD database. All synthetic lines that are deeper than 0.97 of the continuum are identified. A few features not identified are labeled with question marks. Regions where the elimination of strong telluric lines resulted in a degradation of the spectrum are marked with an Earth symbol. In the lower left corner, an enlargement of the spectrum (not shown to scale) is plotted in order to show the fits in greater detail.

invalidity of describing the HFS of the e^6D–w^6F spectrum in terms of A and B hyperfine constants.

6.4. Uncertainties of the gf-values

As it is hard to give any precise values of the *absolute* gf-uncertainties in this work, we focus the current discussion on the *relative* uncertainties. These are undoubtedly also the most relevant quantities to discuss, as the absolute values are easy to rescale with an overall common factor, possibly evaluated from comparison with a well-calibrated measurement. Nevertheless, even though there are few HFS analyses of a complexity comparable to this work, we expect the overall uncertainty of the *absolute* gf-values to be well below 10%.

The uncertainty of the *relative* gf-values can be estimated from comparisons of the synthetic spectra to the corresponding experimental spectra as presented in Figures 2–4. By investigating all hyperfine components of these spectra, one can conclude that the synthetic line, which seems to fit worst with the experimental line, is the leftmost line of Figure 3 at 5765.43 cm^{-1}. This line has a gf-value that is about 10% too small as compared to the experimental, which was noted above in Section 6.2. It should, however, be clear that this is the worst case scenario, as the synthetic spectrum could be scaled up with a factor to better fit this line with the spectrum, and thereby instead overestimate the group of lines in the center of this part of the spectrum. One could therefore consider 10% as an upper limit of the relative gf-uncertainty. Furthermore, it should be noted that this line is an example of a transition that is not at all predicted with a conventional A and B hyperfine constant (or *Diagonal*) analysis. Another line that does not fit perfectly with the experimental spectrum is the structure just to the right of the main peak in Figure 2 at 5770.25 cm^{-1}. The gf-value of this line deviates from the experimental by approximately 5%. Apart from these two lines, we judge the overall uncertainty of the *relative* gf-values to be well within 5%.

7. MODELING STELLAR MN I LINES

A way to test our new calculations of the hyperfine splitting of the Mn lines is to compare with observations of stellar spectra. We have therefore modeled the spectra of the Sun (of spectral type G2V) and of the K1.5 III red giant star Arcturus (α Boo) in the relevant spectral region of 1.73–1.74 μm in order to be able to compare with the atlases of these stars by Livingston & Wallace (1991) and Hinkle et al. (1995a), respectively. The spectral resolution of these atlases is sufficiently high to resolve the stellar spectral lines. We calculated the synthetic spectra

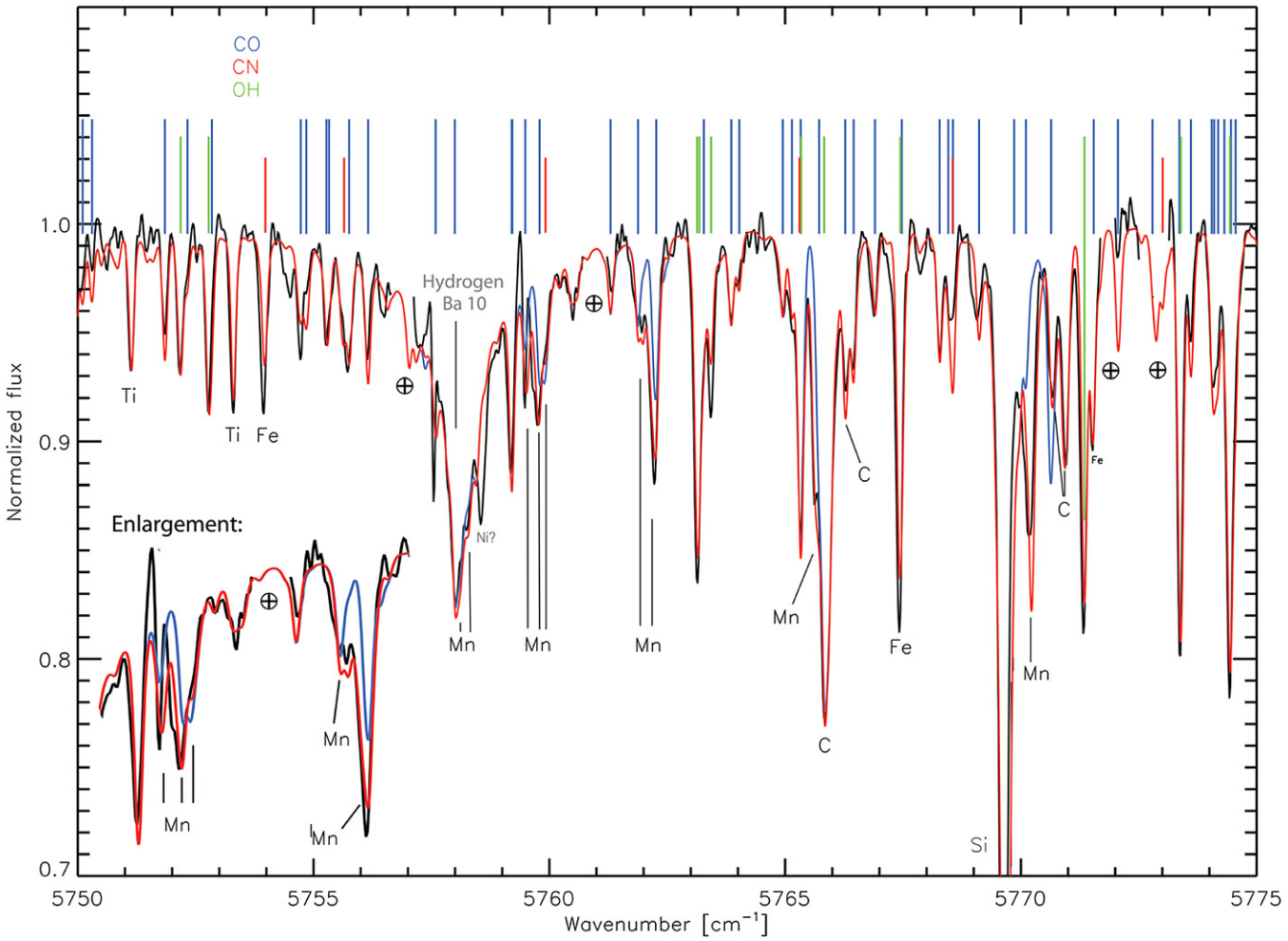

Figure 6. Wavelength region of interest for our newly calculated Mn lines. The observed spectrum of the K1.5 III giant *Arcturus* (Hinkle et al. 1995b) is shown in black and our best synthetic spectrum is shown in red, which includes our newly calculated Mn lines. The blue spectrum shows the spectrum using the Mn line list from the VALD database. All synthetic lines that are deeper than 0.97 of the continuum are identified. Regions where the elimination of strong telluric lines resulted in a degradation of the spectrum are marked with an Earth symbol. In the lower left corner, an enlargement of the spectrum (not shown to scale) is plotted in order to show the fits in greater detail.

for atmospheres modeled with the MARCS code (Gustafsson et al. 2008).[6]

These model atmospheres are hydrostatic and are computed on the assumptions of Local Thermodynamic Equilibrium, chemical equilibrium, homogeneous plane-parallel (for the Sun) or spherically symmetric (for Arcturus) stratification, and conservation of the total flux (radiative plus convective; the convective flux being computed using the local mixing length recipe).

The synthetic spectra were calculated in plane-parallel and spherical symmetry for the Sun and Arcturus, respectively. We sample the spectra with a resolution of $R = 600{,}000$. With a micro-turbulence velocity of 1–2 km s^{-1}, this will ensure adequate sampling. We finally convolve our synthetic spectra, in order to fit the shapes and widths of the observed lines, with a macro-turbulent (and instrumental) broadening, represented by a radial-tangential function Gray (1992), with 2.2 and 3.7 km s^{-1} (FWHM), respectively. The code used for calculating the synthetic spectra is BSYN v. 7.09, which is based on routines from the MARCS code. A $^{12}C/^{13}C$ ratio of 89 is used for the Sun, and 9 for Arcturus; see, e.g., Ryde et al. (2010).

The atomic line list used in our calculations is compiled from the VALD database (Piskunov et al. 1995). When needed, we determined "astrophysical gf-values" by fitting atomic lines in the synthetic spectra to the solar spectrum. The lines fitted were, among others, eight Fe, three C, one Ca, and two Ti lines. In addition, the new strengths ($\log gf$) of the HFS Mn lines are calculated, but are given in a relative scale. The lines fit the best when we scale the strengths by a factor of five. The molecular line lists, which include CO, OH, CN, SiO, and CH, were adopted as they are and instead of modifying the gf-values, the abundances of $\log \epsilon_O = 8.63$ (from OH lines), then $\log \epsilon_C = 8.06$ (from CO lines), and finally $\log \epsilon_N N = 7.67$ (from CN lines) were obtained from the Arcturus atlas, in good agreement with Ryde et al. (2009). For the Sun, a $\log \epsilon_{CNO} = (8.41, 7.80, 8.66)$ abundance is assumed.

In Figure 5, we show our fits to the solar spectrum around the Mn lines by plotting the normalized flux versus frequency given by the wavenumber in cm^{-1}. In this region, the very wide Bracket 10 hydrogen line ($n = 4$–10) dominates and complicates the comparison. The normalization of the flux spectrum in this region is particularly difficult, since the continuum is absent over a wide frequency range due to the hydrogen line.

[6] For the Sun, we use $T_{\rm eff} = 5770$ K, $\log g = 4.44$, $\xi_{\rm micro} = 0.93$ km s^{-1}, and solar abundances, and for Arcturus $T_{\rm eff} = 4280$ K, $\log g = 1.7$, $\xi_{\rm micro} = 1.74$ km s^{-1}, [Fe/H] = −0.53, and [α/Fe] = +0.30; see Ryde et al. (2010) for details.

Furthermore, existing codes calculating the broadening and strengths of solar hydrogen lines cannot fit these lines. We have therefore manipulated the hydrogen opacity by artificially changing the $\log gf$ value for this line in order to fit the local "continuum" when analyzing the Mn lines. The entire spectral region shown in Figure 5 is more or less affected by the hydrogen line. Thus, the original $\log gf = -0.417$ is changed to $\log gf = -0.55$, except for the H-core region, where for the low-frequency side of the Ni line (5756–5757 cm^{-1}) it is changed to $\log gf = -0.75$ and on the high side (5759–5760 cm^{-1}) to $\log gf = -0.65$. The local synthetic spectra thus calculated are shown in the figure. We also show a synthetic spectrum with the original Mn line list (in blue) and compare this to the spectrum calculated with the new one (in red). The new fit is very satisfactory. The Mn lines at 5770 cm^{-1} (17 325 Å) are, however, too strong in the synthetic spectrum compared to the observed spectrum, the reason for which is not understood.

In Figure 6, we present our synthetic fit to the observed spectrum of the cooler giant star Arcturus. We directly see the appearance of the many molecular lines from CO, CN, and OH that dominate the spectrum. The hydrogen line is now more narrow, as expected for a lower-gravity star, with less collisional broadening. The hydrogen line was fitted by changing the opacity through a change in the $\log gf_{\mathrm{HBa10}}$ to −0.7. The general fit to the spectrum of this star is very good, and the synthesized spectrum using the new data of the Mn lines (in red) is particularly an improvement compared with the fit that was possible using previous data (in blue). Again, the Mn lines at 5770 cm^{-1} (17 325 Å) are too strong in the synthesized spectrum, for reasons that require further investigation. We note, however, that these lines lie in the blue wing of a strong Si line, the broadening of which is not accurately synthesized.

As demonstrated in the figures of both the Sun and Arcturus, a few of the Mn lines are nearly absent in the spectra using the old data. For other Mn lines, the residuals between the observed and synthesized spectra have more than halved when using the new data.

8. CONCLUSIONS

We have combined theoretical synthetic and experimental spectra of the $3d^5 4s(^7S)4d$ e^6D – $3d^5 4s(^7S)4f$ w^6F 17325, 17339, 17349, 17357, and 17362 Å lines in Mn I to derive information about the individual hyperfine lines that make up these five spectral features. We have modeled the spectra of the Sun and the red giant star Arcturus using the new atomic data as well as using previously published atomic data, and we have shown that our new data generate a better fit to observed stellar spectra. Using the new HFS data, these lines should therefore be useful in the analysis of stellar spectra.

Due to the extensive number of hyperfine transitions in this system, we have concentrated our discussion on the three strong groups of hyperfine transitions, the 17325, 17339, and 17349 Å lines, and only included the strongest of the transitions of each of these subgroups in the tables of this paper. A complete list of all the individual e^6D – w^6F hyperfine transitions can be found as supporting material.

We have shown that the hyperfine levels involved in these transitions cannot be described in terms of the conventional hyperfine constants. Instead, they have to be described individually due to the large impact of the off-diagonal hyperfine interaction. By fitting our theoretical spectra to experimental ones by allowing for small adjustments to the calculated fine structure energies and hyperfine interaction matrix elements in an iterative procedure, we think we have developed a method that could be applied to similar problems in other atomic and ionic systems of interest to the astrophysical community.

Dr. Paul Barklem is thanked for discussions concerning the modeling of the Hydrogen Ba 10 line and Dr. Kjell Eriksson for valuable help and discussions concerning the running of the MARCS model-atmosphere program. M.A. is financed by the EU under the Science & Technology Fellowship Programme China (STF). J.G. would like to thank the Nordic Centre at Fudan University, Shanghai, for supporting his visit to Fudan in 2013. N.R. is a Royal Swedish Academy of Sciences Research Fellow supported by a grant from the Knut and Alice Wallenberg Foundation. N.R. also acknowledges support from the Swedish Research Council, VR, and Funds from Kungl. Fysiografiska Sällskapet i Lund. EPSRC and PPARC of the UK supported the experimental studies undertaken by R.W.B. while a PhD student at Imperial College London. R.H. and Y.Z. acknowledge the support of the National Natural Science Foundation of China under project No. 11074049 and by the Shanghai Leading Academic Discipline Project B107. P.J. and T.B. acknowledge support from the Swedish research council.

REFERENCES

Abt, A. 1952, ApJ, 115, 199
Andersson, M., & Jönsson, P. 2008, CoPhC, 178, 156
Andersson, M., Jönsson, P., & Sabel, H. 2006, JPhB, 39, 4239
Andersson, M., Lennartsson, T., Nilsson, H., & Chen, C. Y. 2012, JPhB, 45, 135001
Blackwell-Whitehead, R., Pickering, J. C., Pearse, O., & Nave, G. 2005, ApJS, 157, 402
Blackwell-Whitehead, R. J. 2003, PhD thesis, Imperial College, London
Catalan, M. A., Meggers, W. F., & Garcia-Riquelme, O. 1964, JRNBS, 68, A9
Grant, I. P 2007, Relativistic Quantum Theory of Atoms and Molecules: Theory and Computation (Berlin: Springer)
Gray, D. F. 1992, The Observation and Analysis of Stellar Photospheres (2nd ed.; Cambridge: Cambridge Univ. Press)
Grumer, J., Andersson, M., & Brage, T 2010, JPhB, 43, 074012
Gustafsson, B., Edvardsson, B., Eriksson, K., et al. 2008, A&A, 486, 951
Hinkle, K., Wallace, L., & Livingston, W. 1995a, PASP, 107, 1042
Hinkle, K., Wallace, L., & Livingston, W. C. 1995b, Infrared Atlas of the Arcturus Spectrum, 0.9–5.3 microns (San Francisco, CA: ASP)
Jomaron, C. M., Dworetsky, M. M., & Allen, C. S. 1999, MNRAS, 303, 555
Jönsson, P., Gaigalas, G., Bieroń, J., Froese Fischer, C., & Grant, I. P. 2013, CoPhC, 184, 2197
Lide, D. (ed) 2003, CRC Handbook of Chemistry and Physics (84th ed.; Boca Raton, FL: CRC Press)
Livingston, W., & Wallace, L. 1991, An Atlas of the Solar Spectrum in the Infrared from 1850 to 9000 cm^{-1} (1.10 to 5.4 m), NSO Technical Report (Tucson, AZ: National Solar Observatory), 91
Meléndez, J. 1999, MNRAS, 307, 197
Nave, G., Sansonetti, C. J., & Griesmann, U. 1997, OSA Tech. Digest Ser. 3, Fourier Transform Spectroscopy: Methods and Applications (Washington: DC/OSA), 38
Piskunov, N. E., Kupka, F., Ryabchikova, T. A., Weiss, W. W., & Jeffery, C. S. 1995, A&AS, 112, 525
Prochaska, J. X., & McWilliam, A. 2000, ApJ, 537, L57
Ralchenko, Yu., Kramida, A. E., Reader, J., & NIST ASD Team, 2008, NIST Atomic Spectra Database (version 3.1.5), [Online]. Available http://physics.nist.gov/asd3 [2010, February 17]. (Gaithersburg, MD: National Institute of Standards and Technology)
Ryde, N., Edvardsson, B., Gustafsson, B., et al. 2009, A&A, 496, 701
Ryde, N., Gustafsson, B., Edvardsson, B., et al. 2010, A&A, 509, A20
Swensson, J. W. 1966, Die Naturwissenschaften, 53, 330
Taklif, A. G. 1990, PhyS, 42, 69